Cellulose (2022) 29:7703–7720
https://doi.org/10.1007/s10570-022-04731-2

ORIGINAL RESEARCH

# Design and synthesis of waterborne light-responsive cellulose nanocrystal/fluorinated polyacrylate films toward oil/water repellent and self-healing properties

**Jianhua Zhou · Xueli Wang · Xiuqing Liu · Xiang Li**

Received: 9 December 2021 / Accepted: 24 June 2022 / Published online: 23 July 2022


**Abstract** The development of environmentally friendly waterborne polymeric materials is becoming critical today. In this study, a kind of self-healing cellulose nanocrystal/fluorinated polyacrylate based on the reversible photo-induced dimerization of coumarin groups was prepared via RAFT-mediated Pickering emulsion polymerization using cellulose nanocrystal (CNC) particles modified with light-responsive amphiphilic copolymers as Pickering stabilizers. Emulsion polymerization and latex film properties were significantly varied in dependence on the amount of 7-(2-methacryloyloxyethoxy)-4-methylcoumarin (CMA) monomer. Hydrophobic, oleophobic and mechanical properties of the latex film were dynamic in response to UV light. The maximum water contact angle and $CH_2I_2$ contact angle increased by 6.1° and 2.3°on the irradiation of UV light at 365 nm, respectively. The tensile strength of latex film increased initially with increasing amount of CMA increased, from 0 up to 4 wt%, and then decreased. The maximum tensile value increased from 3.0 MPa to 6.4 MPa after the dimerization reaction activated by 365 nm UV light. Results from atomic force microscope (AFM) and energy dispersive X-ray spectrometer (EDX) revealed that latex film possessed a roughness structure and the fluorine had a remarkable enrichment on the film-air interface. Moreover, latex films showed an excellent surface scratch self-healing ability owing to the reversible dimerization reaction of the coumarin groups, and the reversible dimerization reaction of coumarin groups within cellulose nanocrystal/fluorinated polyacrylate polymer was extensively investigated via FT-IR spectrometer and differential scanning calorimetry (DSC). The fruitful outcomes indicated that light-responsive cellulose nanocrystal/fluorinated polyacrylate exhibited a greatly potential application as a smart material.

**Keywords** Fluorinated polyacrylate · Coumarin · Cellulose nanocrystal · Self-healing · Oil/Water repellent

**Supplementary Information** The online version contains supplementary material available at https://doi.org/10.1007/s10570-022-04731-2.

J. Zhou (✉) · X. Wang · X. Liu
College of Bioresources Chemical and Materials Engineering, Shaanxi University of Science and Technology, Xi'an 710021, China
e-mail: zhoujianh@21cn.com

J. Zhou · X. Wang · X. Liu
National Demonstration Center for Experimental Light Chemistry Engineering Education, Shaanxi University of Science and Technology, Xi'an 710021, China

X. Li
College of Chemistry and Chemical Engineering, Shaanxi University of Science and Technology, Xi'an 710021, China

## Introduction

Fluorinated polyacrylate polymers are increasingly investigated owing to their high thermal and chemical resistance, oil and water repellency, transparency, adhesion, and good film-forming, which has made their to be one of the most important polymers used in different fields such as textile, leather, paper making and coating industry (Zhou et al. 2015). Emulsion polymerization has been proven as a fascinating method to obtain fluorinated polyacrylate because water as continuous phase provides a good medium to dissipate the heat of reaction and ensure that the product has a relatively low viscosity, making it easy to handle (Zhou et al. 2014). However, the residual low molecular weight surfactants in a conventional emulsion polymerization have many negative effects, including high toxicity, high environmental pollution, and difficulty in recovery (Zhai et al. 2019). Thus, development of a new type of emulsion polymerization method that can circumvent such above disadvantages is of crucial importance for fluorinated polyacrylate.

Pickering emulsion polymerization, where the solid particles play the role of conventional surfactant, has been developed and exhibit great potential in the latex industry due to the enhanced stability, and fewer particle requirement (Liu et al. 2017). Previous much work on Pickering emulsion polymerization mostly concerns the use of inorganic particles as stabilizers, such as carbon nanotubes (Zhang et al. 2021), silica (Fouconnieret al. 2021), clay (Morgen et al. 2019), and graphene oxide (Hosseinzadeh et al. 2021). However, increasing environmental concerns have led to intense research involving bio-sourced nanoparticles. Among various types of nanoparticles, cellulose nanocrystal (CNC) particles show the advantages of biodegradability, biocompatibility, nontoxicity, high reactivity, low cost, and therefore they have been taken into account as superb stabilizer in Pickering emulsion polymerization. For instance, Zhang et al. (2020) prepared the poly(styrene-co-2-ethylhexyl acrylate) latex particles stabilized with hexyl-functionalized cellulose nanocrystal by the Pickering miniemulsion polymerization. These latexes formed the films that showed much higher storage moduli in the rubbery regime and lower water uptake than those films formed from latexes with sodium dodecyl sulfate (SDS) surfactant. Werner et al. (2019) exploited a novel method to synthesize hybrid polymer materials from O/W Pickering emulsions stabilized by modified CNC particles. Wang et al. (2019a) successfully achieved the controllable preparation of PMMA through metal-free photoinduced electron transfer-atom transfer radical polymerization (PET-ATRP) in Pickering emulsion using CNC particles as stabilizers. Zhang et al.(2019) employed CNC particles as stabilizers to prepare microencapsulation of phase change materials with polystyrene/CNC hybrid shell via Pickering emulsion polymerization. In view of the above benefits, CNC-decorated nanocomposites obtained by Pickering emulsion polymerization exhibit wide and potential applications.

Recently, our group prepared the fluorinated polyacrylate via RAFT-mediated Pickering emulsion using modified CNC particles as stabilizing agents (Zhou et al. 2020; Li et al. 2020).This method not only improves the water and oil repellency of short-chain fluorinated polyacrylate latex film but also solves the problem that CNC particles fall off from the latex surface by covalently anchoring CNC particles on the surface of latex particles. However, we found in the experiment that fluorinated polyacrylate nanocomposites may be susceptible to generate micro notches or breaks from the impact, abrasion and fatigue alone or in combination, which may result in catastrophic failure and shorten their service life. Therefore, the development of fluorinated polyacrylate nanocomposites that can repair cracks on themselves is of vital importance and imperative.

Self-healing polymeric materials have been investigated intensively in the past few years. They have become a kind of promising smart material, which can not only effectively heal the physical damage, but also can extend the lifetime, eliminate potential safety hazards and reduce environmental impact (Cai et al. 2020). Based on the self-healing mechanisms, the self-healing materials fall into two general groups: extrinsic and intrinsic self-healing materials. Researchers have made much effort to construct intrinsic self-healing polymeric materials. Various reversible chemical interactions such as photoresponsive cycloadducts (Abdallh et al. 2019b; Wang et al. 2019b), Diels–Alder adducts (Wei et al. 2020; Yang et al. 2020), disulfide bonds (Guo et al. 2020), acylhydrazone bonds (Zhu et al. 2020) or supramolecular interactions (Lin et al. 2020; Cao et al. 2021) have be mostly used to heal crack. In comparison, the

light-responsive self-healing materials based on photoactive monomer have received increasing attention because of low cost, cleanliness and ease of manufacture (Wang et al. 2019b). Coumarin is an attractive photosensitive monomer because it is capable of photodimerization via [2π + 2π] photocycloaddition with 365 nm UV irradiation and photocleavage upon irradiation at 254 nm (Liu et al. 2020; Moorthy et al. 1992). This property can provide an avenue toward the reversible formation and photolytic cleavage of polymer networks by the light-driven reaction. Therefore, the introduction of the coumarin in a matrix can achieve the formation of light-responsive self-healing materials. Banerjee et al. (2015) prepared the coumarin functionalized polyisobutylene (PIB)-based star polymer, and the polymer films exhibited an excellent self-healing behavior under different wavelengths of ultraviolet (UV) light. Joseph et al. (2020) designed a series of polymers by incorporating photoresponsive coumarin moieties in butyl acrylate based graft copolymers. Polymers showed photo-triggered intrinsic self-healing behavior. Abdallh et al. (2019b) prepared a self-healing polymer film based on coumarin-modified tetrafunctional monomer. Hughes et al. (2019) introduced coumarin groups into epoxy-based network polymers, and the polymer coating showed good self-healing properties under UV light. It can be noticed that in all the above instances, the coumarin as a photoactive monomer has been extensively reported in self-healing hydrogels (Yu et al. 2016), coating and polymer films (Wang et al. 2019b; Wong et al. 2019) but most of these materials were synthesized in an organic solvent medium. In addition, as far as we know, few works have been done to give fluorinated polyacrylate a self-healing function. Consequently, it is an ideal strategy to utilize coumarin as dynamic cross-linker for the synthesis of waterborne fluorinated polyacrylate with self-healing ability.

Herein, we developed a waterborne self-healing fluorinated polyacrylate latex film. In this current work, we introduced the coumarin groups into a fluorinated polyacrylate nanocomposite, which was synthesized through RAFT-mediated Pickering emulsion polymerization using light-responsive amphiphilic block copolymer modified cellulose nanocrystal (PAA-*g*-CNC-*g*-P(HFBA-*co*-CMA)) particles as Pickering stabilizers, and the coumarin as photoactive moieties. It is worth noting that the designed light-responsive cellulose nanocrystal/fluorinated polyacrylate was not only easy to improve hydrophobic and oleophobic properties of short-chain fluorinated polyacrylate latex film but also can endow the latex film with self-healing property. Furthermore, the element composition, water–oil repellent, mechanical and self-healing properties were systematically studied, respectively.

## Experimental

### Materials

Glycidyl methacrylate (GMA) and dimethylaminopyridine (DMAP) were purchased from Shanghai Aladdin Reagent Co., Ltd. (China). 4,4-Azobis(4-cyanopentanoic acid) (V501) was obtained from Fluka Company (Buchs, Switzerland). Cellulose nanocrystal (CNC) was purchased from the University of Maine (America). Potassium persulfate (KPS) was purchased from Tianjin Tianli Chemical Reagent Co., Ltd. (China). The light-responsive cellulose nanocrystal/fluorinated polyacrylate latex particles were synthesized by emulsion polymerization with monomers butyl acrylate (BA), methyl methacrylate (MMA), 7-(2-methacryloyloxyethoxy)-4-methylcoumarin (CMA), and hexafluorobutyl acrylate (HFBA). BA and MMA monomers were supplied by Tianjin Kemiou Chemical Reagent Co., Ltd. (China). CMA monomer was synthesized as described in Ref. (Kabb et al. 2018; Zhang et al. 2017) and its $^{1}$H-NMR spectrum is seen in Figure S1. HFBA monomer was provided by Harbin Xuejia Fluorosilicide Co., Ltd. (China). BA, MMA, and HFBA monomers were purified by passing through an inhibitor remove column. PAA-RAFT was synthesized as described in Ref. (Zhou et al. 2016).

### Synthesis of PAA-b-PGMA-b-P(HFBA-co-CMA)

PAA-RAFT (3.0257 g), GMA (0.7953 g), V501 (0.0314 g), and 1, 4-dioxane (38 mL) were weighed into a flask and degassed with argon gas for 30 min. The mixture was then heated to 60℃. After reaction for 6 h, the resulting product was then purified by precipitation into n-hexane. After being dried under vacuum for 12 h, the poly(acrylic acid)-*b*-poly(glycidyl methacrylate) (PAA-*b*-PGMA-RAFT) could be

obtained, which would be used as a macro-chain transfer agent in the following polymerization. The $^{1}$H-NMR spectrum and GPC curve of PAA-*b*-PGMA-RAFT are shown in Figure S2 and Figure S3.

The PAA-*b*-PGMA-RAFT (2.1922 g), HFBA (0.7579 g), CMA (0.4622 g), and V501 (0.0225 g) were dissolved in 1, 4-dioxane (30 mL) by intense stirring. After purging the mixture solution with argon gas for 30 min, the polymerization reaction was carried out at 80℃ for 8 h. The product was precipitated in n-hexane and dried in vacuum. Finally, the poly(acrylic acid)-*b*-poly(glycidyl methacrylate)-*b*-poly (hexafluorobutylacrylate-*co*-7-(2-methacryloyloxyethoxy)-4-methylcoumarin) (PAA-*b*-PGMA-*b*-(HFBA-*co*-CMA)) was obtained.

## Preparation of light-responsive cellulose nanocrystal

CNC (1.13 g) and PAA-*b*-PGMA-*b*-P(HFBA-*co*-CMA) (3.26 g) were dispersed in 106 mL of N, N-dimethylformamide (DMF) with an ultrasonic cell pulverizer, and then the mixture was added to a flask. The DMAP (0.23 g) was added into the flask. The flask was submerged in an oil bath at 50℃, and the mixture was magnetically stirred. After 24 h, the product light-responsive cellulose nanocrystal PAA-*g*-CNC-*g*-P(HFBA-*co*-CMA) (MCNC) was collected by centrifugation and then washed 3 times by the same procedure with tetrahydrofuran (THF) as wash solvent. Finally, the product could be obtained after overnight at 50 °C under a vacuum.

## Preparation of light-responsive cellulose nanocrystal/fluorinated polyacrylate emulsion

Light-responsive cellulose nanocrystal/fluorinated polyacrylate emulsion was prepared by polymerizing the mixed monomers (BA/MMA/HFBA/CMA) inside latex particles using PAA-*g*-CNC-*g*-P(HFBA-*co*-CMA) (MCNC) particles as Pickering stabilizers. The synthesis recipes were listed in Table 1. In a typical process, PAA-*g*-CNC-*g*-P(HFBA-*co*-CMA) particles (0.10 g) were evenly dispersed in distilled water (34 mL) with pH value of 13 via ultrasonication to form PAA-*g*-CNC-*g*-P(HFBA-*co*-CMA) aqueous dispersion. Thereafter, HFBA (1.00 g), BA (7.12 g), MMA (1.78 g), and CMA (0.10 g) were added into the PAA-*g*-CNC-*g*-P(HFBA-*co*-CMA) aqueous dispersion, followed by ultrasonication for 10 min to form the Pickering emulsion. 1/3 KPS aqueous (0.12 g in 6 mL deionized water), and 1/4 Pickering emulsion were then added to a round-bottom flask. The reacting mixture was deoxygenated with argon gas for 30 min and then heated at 65 °C for 30 min. Afterwards, both the remnant KPS aqueous and remnant Pickering emulsion were dropwisely added into the reacting mixture at 80 °C for 90 min. The emulsion was polymerized at 80 °C for 2 h.

## Preparation of latex film

A predetermined amount of light-responsive cellulose nanocrystal/fluorinated polyacrylate emulsions were poured into the cleaned silicone mold. The latex films were formed at room temperature for 48 h, and then dried under vacuum at 80℃ for 3 h to remove water inside the film, followed by annealing in a 120℃ vacuum oven for 30 min. The thickness of the prepared films was 0.5 ~ 0.6 mm.

## Characterization

The fourier transforms infrared (FT-IR) spectra were performed on a BRUKER FT-IR spectrometer

**Table 1** Experimental conditions for the preparation of light-responsive cellulose nanocrystal/fluorinated polyacrylate emulsion

| Sample | S1 | S2 | S3 | S4 | S5 | S6 |
|---|---|---|---|---|---|---|
| PAA-*g*-CNC-*g*-P(HFBA-*co*-CMA)/g | 0.10 | 0.10 | 0.10 | 0.10 | 0.10 | 0.10 |
| KPS/g | 0.12 | 0.12 | 0.12 | 0.12 | 0.12 | 0.12 |
| MMA/g | 1.78 | 1.78 | 1.78 | 1.78 | 1.78 | 1.78 |
| BA/g | 7.12 | 7.12 | 7.12 | 7.12 | 7.12 | 7.12 |
| HFBA/g | 1.00 | 1.00 | 1.00 | 1.00 | 1.00 | 1.00 |
| CMA/g | 0.00 | 0.10 | 0.20 | 0.30 | 0.40 | 0.50 |
| Distilled water/mL | 40.00 | 40.00 | 40.00 | 40.00 | 40.00 | 40.00 |

(VERTEX 70) equipped with an ATR accessory in the range of 4000–400 $cm^{-1}$. $^1$H-NMR spectrum was measured on a Bruker 600 MHz spectrometer (AVANCE NEO) using dimethyl sulfoxide-$d_6$ (DMSO-$d_6$) as solvent. The morphology of sample was obtained on a transmission electron microscope (TEM, Tecnai G2-F20 S-TWIN) at a voltage of 200 kV. The molecular weight and molecular weight distribution of samples were performed on the gel permeation chromatography (GPC, Waters e2695) equipped with a refractive index detector. A solution of LiBr (10 mM) in dimethylformamide (DMF) was used as the mobile phase at a flow rate of 0.8 mL/min. The thermal properties of samples were evaluated with the thermogravimetric analysis (TGA, TGA Q500). The samples were heated from 0 °C to 800 °C at a heating rate of 10℃/min in a nitrogen atmosphere. The crystal structure of the CNC and MCNC was measured on a BRUKER X-ray diffractometer (D8 Advance) with a Cu Kα radiation source energized at 40 kV. All samples were power and contained in the holder of 10 mm dimeter and 1 mm thickness. Measurements were collected in the 2θ range from 10° to 50° at a rate of 2°/min. The measurement resolution was 0.05°. All the measurements were carried out at least in duplicates. Firstly collecting the blank run data and then subtracting it from the experimental data of the sample. The software of MDI Jade and Origin were used to process the XRD curve. Monomer conversion and gel rate were obtained through the use of gravimetry. Dynamic light scattering (Malvern Zetasizer Nano) was applied to measure the particle size and particle size distribution of the latex particles at 25℃. The hydrophobic and oleophobic properties of the latex film were evaluated by measuring the contact angle of small water or diiodomethane drop using a contact angle analyzer (DCA-20). Atomic force microscopy (AFM) was performed in a tapping mode to obtain the microscopic morphology of latex films. Tensile tests were performed at 25 ℃ on dumbbell-shaped specimens (thickness: 0.5 ~ 0.6 mm, length and width of narrow parallel portion: 15 mm and 2 mm) according to ISO527-2 using a tensile testing machine (AI-7000-NGD) equipped with a 500 N load cell. Three samples were tested per film. Elemental analysis of the latex films was studied using an energy dispersive X-ray analysis (EDX, Hitachi JEOL-JSM-6700F system, Japan), which is an attachment to the scanning electron microscopy (Hitachi S-48000). The differential scanning calorimetry (DSC) of the sample was used to evaluate glass transition temperature ($T_g$), which was performed on a differential scanning calorimeter (DSC Q2000) at a heating rate of 10 ℃/min from -80 °C to 200 °C under nitrogen atmosphere. The self-healing behaviour of the scratches on latex film surface was observed by a visual inspection. The latex films were scratched by a razor blade after an irradiation at 365 nm. Subsequently, the latex films were firstly irradiated with UV light of 254 nm for promoting the photo cleavage process and then irradiated at 365 nm at 100 °C on a heating plate to achieve healing of the scratches. The morphology of each sample was monitored using a 3D ultra-depth-of-field microscope (KH8700).

## Results and discussion

### Preparation of light-responsive cellulose nanocrystal

Light-responsive cellulose nanocrystal PAA-*g*-CNC-*g*-P(HFBA-*co*-CMA) (MCNC) particle was prepared by chemically grafting PAA-*b*-PGMA-*b*-P(HFBA-*co*-CMA) onto cellulose nanocrystal (CNC) (Scheme 1). The PAA-*b*-PGMA-*b*-P(HFBA-*co*-CMA) was prepared by reversible addition fragmentation chain transfer (RAFT) polymerization, and its structure and composition were analyzed by $^1$H-NMR spectroscopy and gel permeation chromatography (GPC). Figure 1 displays the $^1$H-NMR spectrum of the PAA-*b*-PGMA-*b*-P(HFBA-*co*-CMA). The characteristic signals of the PAA segment appear at 2.22 ppm(-C<u>H</u>(COOH)$CH_2$-) and 12.23 ppm(-COO<u>H</u>)). The peak at 6.03 ppm(-C<u>H</u>F-) is ascribed to the PHFBA segment. The characteristic signals at 7.68 ppm (-CH-C<u>H</u>-C-), 7.01 ppm(-O-C–C<u>H</u>-, -O–C<u>H</u>-C-), 6.20 ppm(-C-C<u>H</u>$_2$-CO), and 2.39 ppm(-C-C<u>H</u>$_3$) belong to PCMA segment. The characteristic peaks of (-O–C<u>H</u>-$CH_2$-) and (-CH-C<u>H</u>$_2$-O-) in PGMA segments appear at 2.70 ~ 2.90 ppm and 3.74 ppm, respectively. Figure 2 is the molecular weight and polydispersity (PDI) for the PAA-*b*-PGMA-*b*-P(HFBA-*co*-CMA). The GPC chromatogram shows the $M_n$ of the PAA-*b*-PGMA-*b*-P(HFBA-*co*-CMA) is $1.45 \times 10^4$ g/mol, and the PDI is 1.10. The low PDI of the PAA-*b*-PGMA-*b*-P(HFBA-*co*-CMA) confirmed the well controllability of RAFT polymerization technique. These results

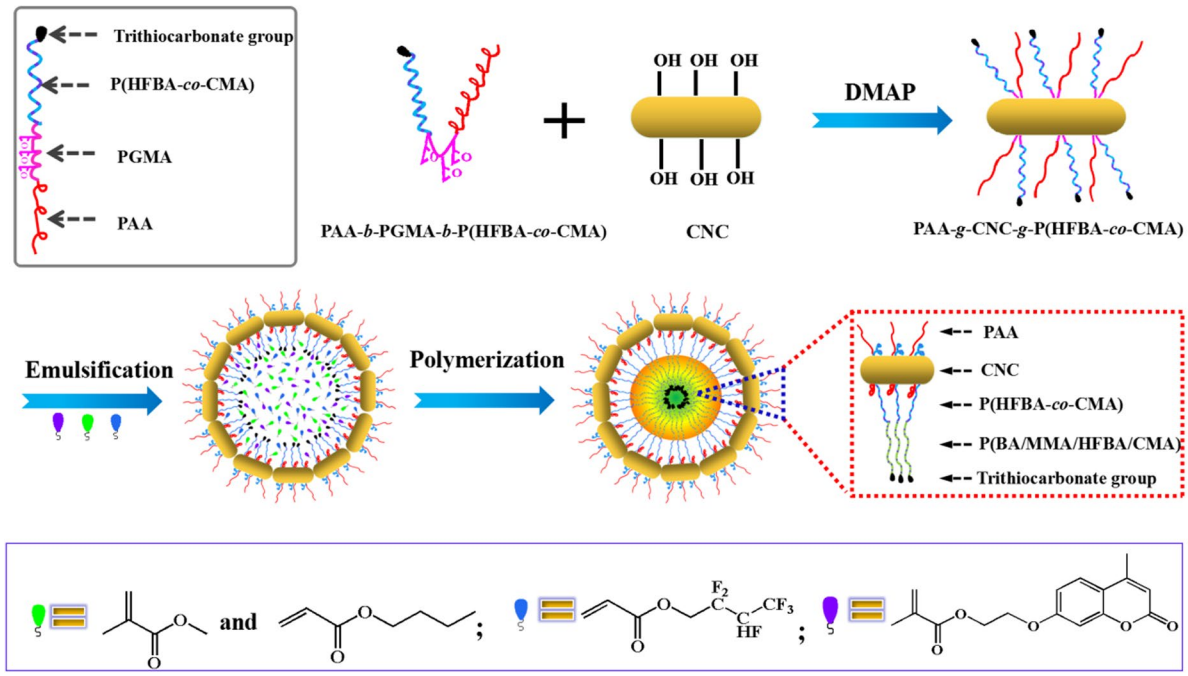


**Scheme 1** Reaction scheme for light-responsive cellulose nanocrystal/fluorinated polyacrylate

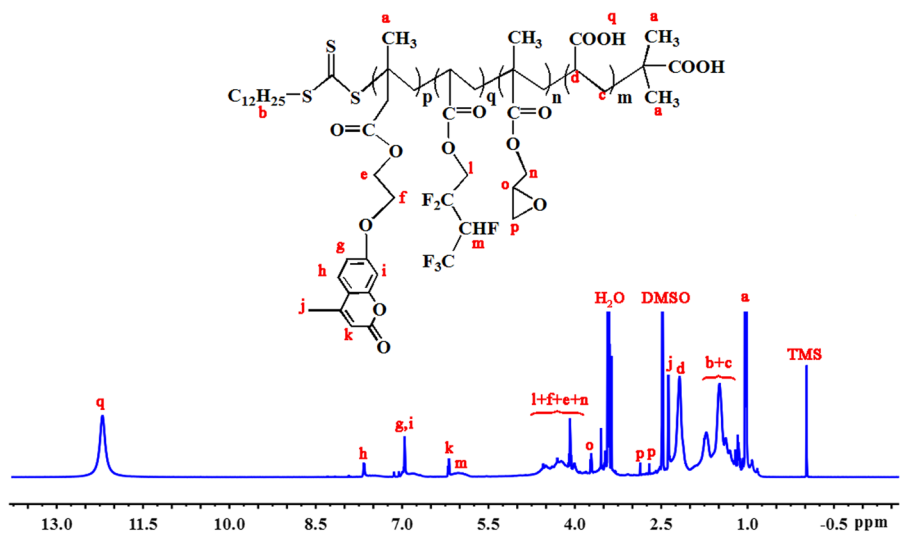


**Fig. 1** $^{1}$H-NMR spectrum of PAA-*b*-PGMA-*b*-P(HFBA-*co*-CMA)

show that the PAA-*b*-PGMA-*b*-P(HFBA-*co*-CMA) is successfully synthesized.

The structure and composition of the original CNC and the MCNC were characterized by FT-IR, TEM, XRD, and TG. Figure 3a shows the FT-IR spectra of CNC and MCNC. In the FT-IR spectrum of CNC, the absorption band at 3350 $cm^{-1}$ is related to O–H stretching vibration, and the band at 2900 $cm^{-1}$ is attributed to C-H stretching vibration. The band in the range of 1420–1430 $cm^{-1}$ comes from the -$CH_2$ bending vibration. The band located at 1054 $cm^{-1}$, corresponds to the C–O–C pyranose ring stretching vibration, and bands occurring at 900–890 $cm^{-1}$ result from the cellulosic β-glycosidic linkage (Bonardd

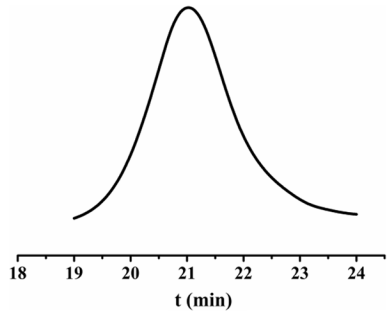


**Fig. 2** GPC trace of the PAA-*b*-PGMA-*b*-P(HFBA-*co*-CMA)

et al. 2018). On the contrary, the FT-IR spectrum of MCNC shows two strong absorption bands. The band at 1568 $cm^{-1}$ corresponds to the coumarin group, and the C=O stretching vibration of PAA-*b*-PGMA-*b*-P(HFBA-co-CMA) polymer is observed at 1729 $cm^{-1}$. In addition, 1190 $cm^{-1}$ ~ 1210 $cm^{-1}$ is assigned to the asymmetric stretching vibration of C-F in -$CF_2$- and -$CF_3$. These results demonstrate that light-responsive cellulose nanocrystal PAA-*g*-CNC-*g*-P(HFBA-*co*-CMA) is synthesized successfully.

Figure 3b shows the TEM images for the CNC and MCNC. It can be found that both CNC and MCNC appear as needlelike particles with dimension of 100 ~ 200 nm in length and 5 ~ 10 nm in diameter. Compared with CNC, after PAA-*b*-PGMA-*b*-P(HFBA-*co*-CMA) polymer modification, the MCNC particles have uniform morphology and contain PAA-*b*-PGMA-*b*-P(HFBA-*co*-CMA) polymer evenly distributed over the whole surface. In addition, it can be seen that the morphology of CNC after grafting polymer was not apparently destroyed.

The XRD patterns of CNC and MCNC are displayed in Fig. 3c. From this figure, CNC and MCNC show similar diffraction peaks. A broad hump-like peak at 2θ = 14°-18° can be assigned to the (1–10) and (110) crystal planes of cellulose I. And a weak peak at 2θ = 12.3° for (1–10) plane is characteristic for cellulose II crystal. The diffraction peak at 20.5° is superimposed with the (102) and (012) reflections of cellulose I and the (110) reflection of cellulose II. The strong peak at 22.4° can be attributed to the (200) crystal plane of cellulose I and the (020) crystal plane of cellulose II, and the peak at 34.8° coincides with the (004) crystal plane of cellulose I and cellulose II (French 2013; Bian et al. 2017; Yue et al. 2015; Xu et al. 2013). The results show that cellulose I and cellulose II coexist in cellulose nanocrystals (Yue et al. 2015; Xu et al. 2013), and the crystalline structure of cellulose is not changed during the grafting reaction.

Thermal stability of CNC and MCNC was measured by the thermogravimetric method. The TG and differential thermogravimetric (DTG) curves of the samples are shown in Fig. 3(d). Both the CNC and

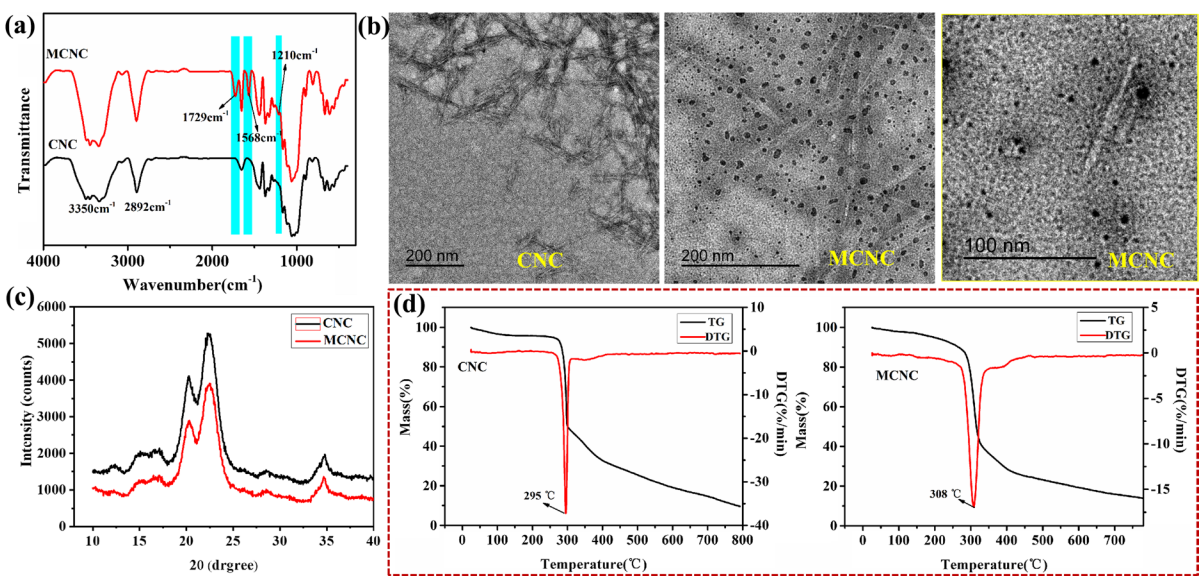


**Fig. 3** **a** FT-IR spectra, **b** TEM images, **c** XRD images and **d** TG and DTG curves of CNC and MCNC

MCNC display a similar degradation behavior. The maximum thermal decomposition temperature of MCNC (308 °C) is higher than that of CNC (295℃), indicating that the thermal stability of cellulose nanocrystal modified by PAA-*b*-PGMA-*b*-P(HFBA-*co*-CMA) polymer has been improved, which is attributed to the high C-F bond energy of PHFBA segment in PAA-*g*-CNC-*g*-P(HFBA-*co*-CMA).

## Synthesis and characterization of light-responsive cellulose nanocrystal/fluorinated polyacrylate

Light-responsive cellulose nanocrystal/fluorinated polyacrylate emulsion was obtained via RAFT-mediated Pickering emulsion polymerization using MCNC particles as stabilizers. As illustrated in Scheme 1, the MCNC contains the hydrophilic PAA segment and hydrophobic P(HFBA-*co*-CMA) segment with reactive trithiocarbonate end group, which can self-assemble at the oil–water interface, acting as surfactant to form the stable Pickering emulsion. Thereafter, the composite emulsion is synthesized through polymerizing the mixed monomers (BA/MMA/HFBA/CMA) inside the latex particles under RAFT control throughout the process due to the active RAFT end located in the latex particle interior. Ultimately, MCNC particles are covalently grafted onto the latex particles surface.

As a functional monomer, the dosage of the CMA monomer is very important for the stability of emulsion polymerization and the properties of latex film. Thus, it is of great significance to explore the effect of CMA dosage on emulsion polymerization. The results of polymerization reaction carried out in different CMA dosages are given in Fig. 4. With the increase of the CMA dosage from 0 to 5 wt%, the monomer conversion which has a connection with emulsion stability increases gradually, as shown in Fig. 4. The gel rate and particle size distribution gradually decreases with the increase of CMA dosage, while the particle size of approximately 337 nm does not change considerably. The reason for this phenomenon is that PAA-*g*-CNC-*g*-P(HFBA-*co*-CMA) particles are used as Pickering stabilizers in polymerization process. PCMA segment in P(HFBA-*co*-CMA) segment has a good compatibility with CMA monomers, which makes it more easily diffuse into the micellar interior and participate in polymerization. In the absence of CMA monomers, due to the bad compatibility between mixed monomers and P(HFBA-*co*-CMA) segments, the emulsion is not stable during the polymerization process, giving rise to a high gel rate. With an increase in CMA dosage, the CMA

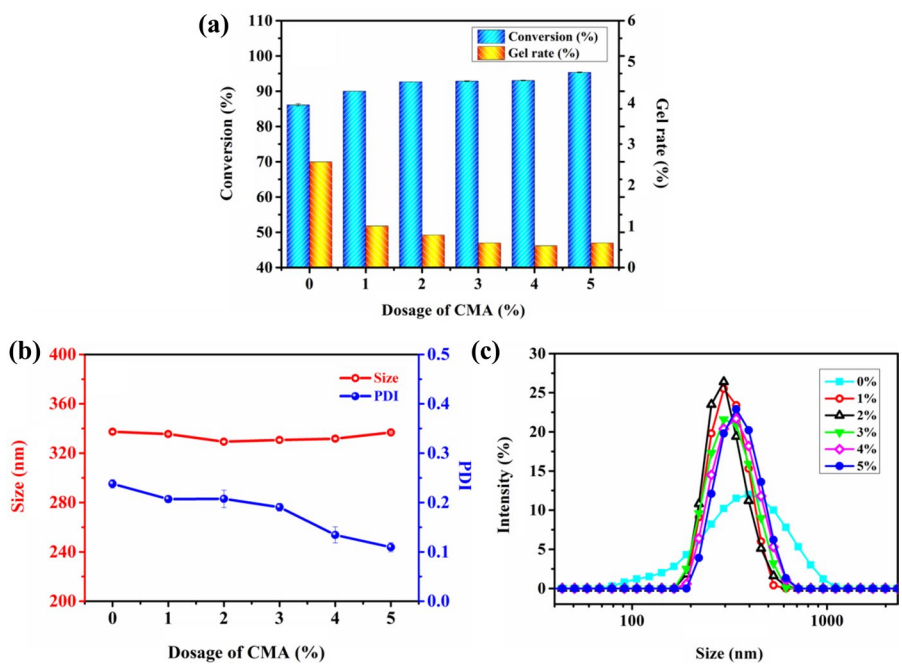


**Fig. 4** Effect of CMA dosage on the monomer conversion, gel rate (**a**), latex particle size (**b**), and particle size distribution (**c**)

monomers diffuse into the micellar interior, the solubilization effect of micelles on monomer is enhanced, which improves the compatibility of CMA monomer with other monomers. In this case, a stable polymerization process is prone to form (Li et al. 2020), resulting in the increase of monomer conversion, and the decrease of gel rate and the particle size distribution.

TEM and FT-IR spectroscopy were performed to verify the successful synthesis of light-responsive cellulose nanocrystal/fluorinated polyacrylate. Figure 5a shows the TEM image of the latex particles. It is obviously shown that most of the latex particles are well-shaped as a regular sphere, the diameter of which is approximately 60 nm. The gray region located inside the composite particles is fluorinated polyacrylate polymer, and the dark region around composite latex particles is MCNC particles. In addition, all latex particles have a well-defined core–shell structure and the thickness of MCNC particle layer is more uniform, which indicates that MCNC particles are dispersed and precisely self-assembled at water-in-oil interface, playing a solid surfactant role. Furthermore, the diameter of the latex particles determined from the TEM data is smaller than the diameter of the same latex particles measured by DLS (335 nm in Fig. 4b). This apparent discrepancy results from the shrinkage of the latex particles when dried before TEM analysis. Figure 5b exhibits the FT-IR spectrum of light-responsive cellulose nanocrystal/fluorinated polyacrylate. The peaks at 1723 $cm^{-1}$ and 1154 $cm^{-1}$ correspond to -C=O and -C-O- stretching vibration, respectively. The band at 1234 $cm^{-1}$ results from C-F stretching vibration, and the peak at 1575 $cm^{-1}$ belongs to the coumarin groups. The -CH stretching vibration bands of $-CH_3$ and $-CH_2-$ appear at 2869 $cm^{-1}$ and 2953 $cm^{-1}$, and its bending vibration bands appear at 1381 $cm^{-1}$ and 1453 $cm^{-1}$. These results demonstrate that the mixed monomers (BA/MMA/HFBA/CMA) involved in reaction were successfully polymerized and the formation of light-responsive cellulose nanocrystal/fluorinated polyacrylate.

## Hydrophobic and oleophobic properties of the latex film

The hydrophobic and oleophobic properties of the latex film surface are mainly determined by its chemical composition and surface roughness (Zhou et al. 2013). In our system, 7-(2-methacryloyloxyethoxy)-4-methylcoumarin (CMA) is used as a hydrophobic photo-sensitive monomer to prepare light-responsive cellulose nanocrystal/fluorinated polyacrylate. Thus, the CMA dosage and photo-dimerization of coumarin moieties maybe have a significant influence on the hydrophobic and oleophobic properties of cellulose nanocrystal/fluorinated polyacrylate latex film.

Contact angle measure was used to explore the effect of CMA dosage on hydrophobic and oleophobic properties of the latex film surface. As seen in Fig. 6, with the increase of dosage of CMA, the water contact angle gradually increases, while the $CH_2I_2$ contact angle does not change much. Because the PCMA has no oleophobicity for the nonpolar liquids, so the dosage of CMA has little effect on the $CH_2I_2$ contact angle. In addition, we find that the contact angle increases after irradiation at 365 nm, and the maximum water contact angle and $CH_2I_2$ contact

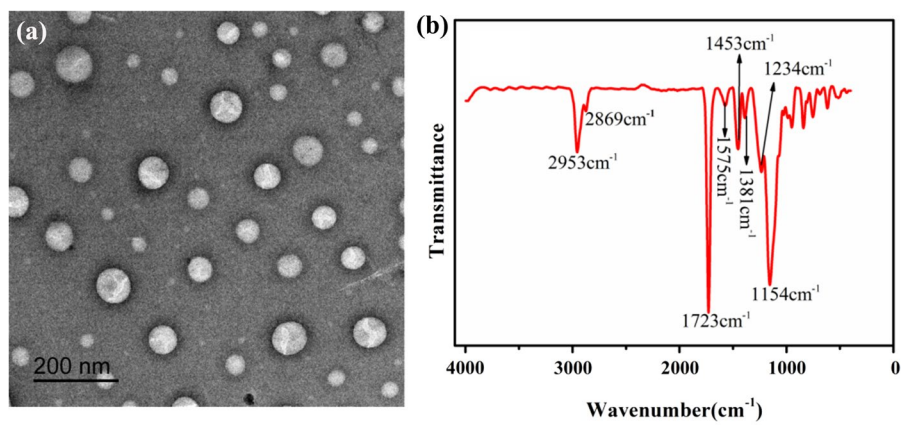


**Fig. 5** TEM image (**a**) and (**b**) FT-IR spectrum for light-responsive cellulose nanocrystal/fluorinated polyacrylate latex particle

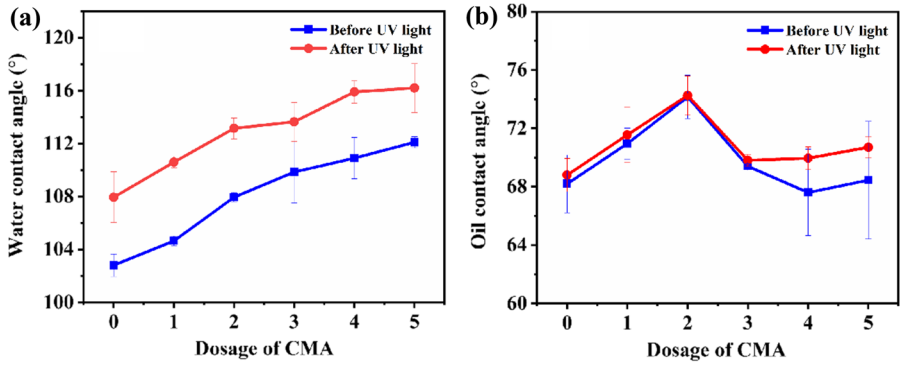


**Fig. 6** Water (**a**) and $CH_2I_2$ (**b**) contact angle of latex films with different CMA dosages before and after illumination at 365 nm UV light

angle increases by 6.1° and 2.3°, respectively. Two explanations can be proposed to account for this phenomenon. Firstly, the crosslinking density of the latex film increases along with the increase of CMA dosage due to the photodimerization of the coumarin groups (Banerjee et al. 2015). Secondly, the interesting improvement of the hydrophobic and oleophobic properties is due to the greater roughness of latex film after 365 nm UV irradiation according to the result obtained by AFM (Fig. 7), and the lower surface free energy of latex film induced by the migration of fluorine atoms under the action of heat generated by light. As presented in Fig. 7, both of the latex films before and after irradiation at 365 nm have a rougher surface. Compared with the original latex film, after the UV irradiation of 365 nm, the roughness of the latex film is further improved, and average roughness (Ra) increases from 5.61 nm to 6.17 nm (Table 2). This result indicates the UV irradiation can change the microstructure morphologies of latex film. A rational explanation is that when irradiated with 365 nm UV light, the PCMA parts of the polymer molecular chains on the PAA-*g*-CNC-*g*-P(HFBA-*co*-CMA) particles occur [2π + 2π] ring dimer reaction, which will cause the cellulose nanocrystal to aggregate in the film and the hierarchical structures are formed to improve the surface roughness. As a result, when the rough surface comes into contact with water/oil, air trapping in the rough area may occur, which will improve greatly the hydrophobicity and oleophobicity (Han et al. 2014). In addition, the water contact angle of the latex film with 0% CMA changes from 102.8° to 108.0° after 365 nm UV irradiation because there is a small amount of PCMA segments on MCNC.

The surface properties have a close relationship with the surface chemical composition of the material. Energy dispersive X-ray spectrometer (EDX) is a rapid analytical technique and can be used to analyze the surface chemical composition of cellulose nanocrystal/fluorinated polyacrylate latex film. Figure 8 presents the EDX results of latex film. According to the result, F element content of 7.18%, 6.57%, 6.44% are observed for the film-air interface, film section and film-glass interface, respectively, which strongly suggests that the fluorine element presents a gradient distribution along the depth direction (Zhou et al. 2013). This can be explained by the fact that lots of $-CF_2$ and $-CF_3$ groups can be spontaneously enriched on the surface-air interface during heating treatment, and then spread and occupy the film surface, reducing the surface free energy of the latex film (Zhou et al. 2015). The combination of the rough surface constructed by cellulose nanocrystal particles and the low surface energy provided by fluorinated polymers improves the hydrophobic and oleophobic properties of latex film.

## Mechanical properties of the latex film

Tensile testing was used to monitor the mechanical properties of the latex film before and after UV treatment. Figure 9 shows the mechanical properties for all film samples, and they exhibit marked differences in tensile strength and the elongation at break before and after 365 nm UV light irradiation. Before 365 nm irradiation, the elongation at break decreases as the dosage of CMA increases, while tensile strength increases as the dosage of CMA increases from 0 to 4wt %, and decreases afterwards with further increase in the CMA dosage. CMA containing a substituted benzene ring has a more rigid structure. Therefore, the increase of its

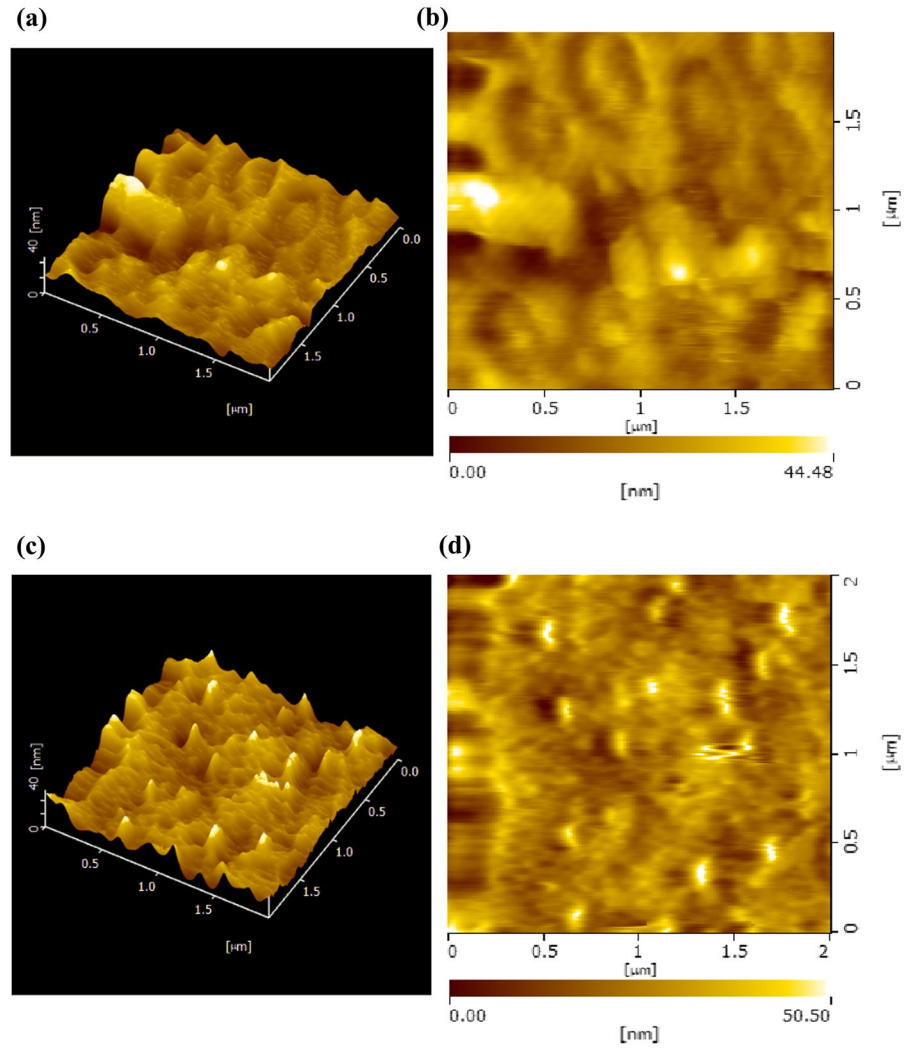


**Fig. 7** AFM images of light-responsive cellulose nanocrystal/fluorinated polyacrylate latex film before (**a**, **b**) and after (**c**, **d**) irradiation at 365 nm UV light

**Table 2** The surface roughness parameters of light-responsive cellulose nanocrystal/fluorinated polyacrylate latex film before (a) and after (b) irradiation at 365 nm UV light

| Sample | Ra (nm) | Rz (nm) | RMS (nm) |
|---|---|---|---|
| Non-irradiation | 5.61 | 36.04 | 7.23 |
| Irradiation at 365 nm | 6.17 | 52.67 | 7.94 |

dosage make more rigid domains produce, which makes the polymer molecular chain more difficult to move. Thus the tensile strength increases and the elongation at break decreases. However, when the CMC dosage is more than 4 wt%, the degree of freedom of polymer molecules is too low, and the mutual diffusion and permeability between adjacent macromolecular segments decrease, which may cause brittleness of the hybrid film, resulting in the decline of mechanical properties. Surprisingly, the mechanical properties of latex film undergo significant variations with a 365 nm UV light irradiation. As depicted in Fig. 9b, the tensile strength of all latex films increases, and the maximum tensile value for the latex film containing 4 wt% CMA increases from 3.0 MPa to 6.4 MPa after exposure to 365 nm UV light. The increase of the tensile strength is attributed to the generation of the chemical cross-linking network owing to the dimerization between the coumarin groups in PCMA segment, thus preventing polymer molecular chains from moving, endowing latex film with rigid structure, and enhancing the film mechanical property

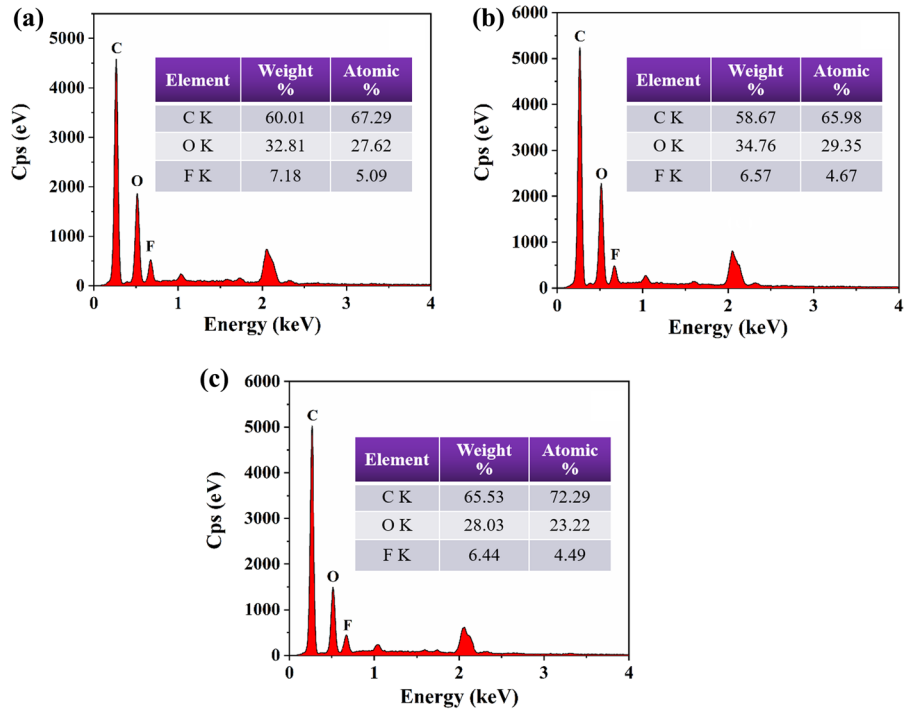


**Fig. 8** EDX spectra and the element mapping of film-air interface (**a**), film section(**b**) and film-glass interface (**c**) of light-responsive cellulose nanocrystal/fluorinated polyacrylate latex film

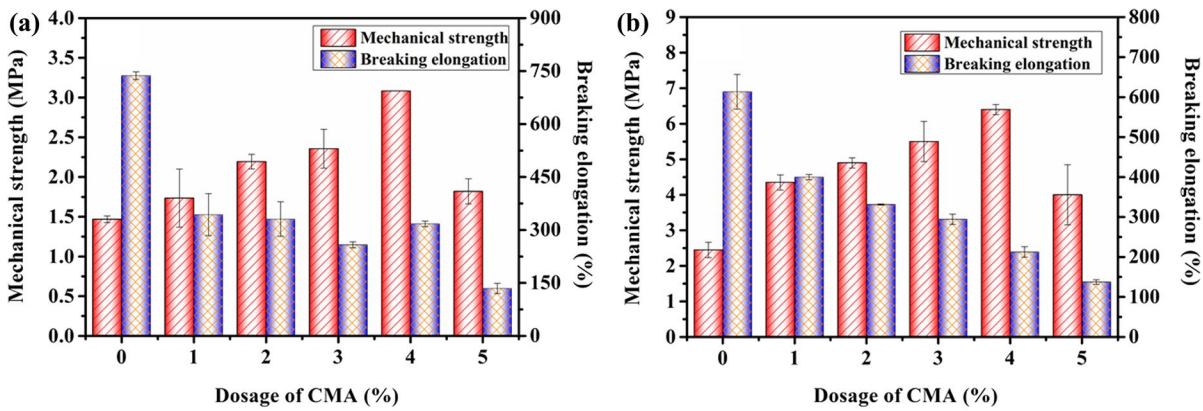


**Fig. 9** Effect of CMA dosage on mechanical properties of latex film before (**a**) and after (**b**) irradiation with 365 nm UV light

(Navarro et al. 2020). In addition, after 365 nm UV irradiation, the tensile strength of the latex film with 0% CMA increases from 1.5 MPa to 2.4 MPa, and the elongation at break decreases from 737.1% to 613.4%. Since the MCNC contains P(HFBA-co-CMA) blocks, the coumarin groups on the PCMA segment can also undergo photodimerization after UV irradiation at 365 nm, so the mechanical properties of the latex film with 0% CMA also change.

## Self-healing behaviors of the latex film

The reversible photochemical reaction of the coumarin moieties is very significant for healing of our system. The dimerization and cleavage reactions from coumarin moieties are demonstrated by FT-IR spectroscopy (Fig. 10). It should be noted that the irradiated latex film at 254 nm in FT-IR spectrum has been represented in red. Compared with the spectrum of

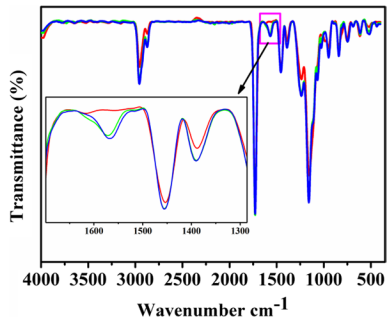


**Fig. 10** FT-IR spectra of light-responsive cellulose nanocrystal/fluorinated polyacrylate latex film before irradiation (blue), after depolymerisation irradiation with 254 nm (red), and after repolymerization irradiation with 365 nm (green)

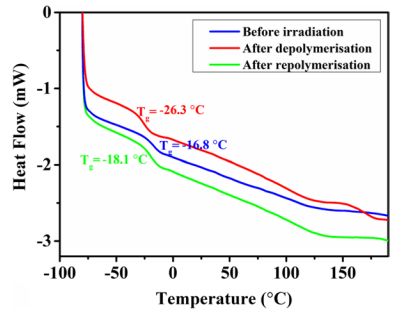


**Fig. 11** DSC curves of latex film: before irradiation (blue), after depolymerisation irradiation with 254 nm (red) and after repolymerization irradiation with 365 nm (green)

sample (irradiation at 365 nm), the most evident signal at 1575 $cm^{-1}$ for the coumarin dimers can be seen to disappear, and two small peaks at 1558 $cm^{-1}$ and 1616 $cm^{-1}$ appear, which indicates that the cyclobutene structure was destroyed because these peaks originate from the carbon–carbon double bonds of the coumarin (Hughes et al. 2019). After further irradiation with 365 nm UV light, it is observed that the peak at 1575 $cm^{-1}$ appears again. FT-IR results confirm that the coumarin moieties successfully undergo a reversible reaction under UV irradiation (Obi et al. 1999). Although the intensity of the peak is largely recovered, this recover is not complete, indicating with not all coumarin groups can reform cyclobutane rings. This may be owing to the misalignment of some coumarin moieties resulting from the restricted mobility of the polymer chain and the lack of adequate approach of the coumarin groups (Abdallh et al. 2017; Hughes et al. 2018).

In order to further obtain information regarding the molecular cleavage/reformation reversibility in polymer chain, and to gain an insight into the self-healing mechanism of latex film, DSC was performed to measure the $T_g$ of the latex film with 3% CMA dosage. The $T_g$ values before and after irradiation were provided, as shown in Fig. 11. Compared to the $T_g$ value (-16.8℃) of the original sample (irradiation at 365 nm), the DSC curve obtained after irradiation with 254 nm UV light shows a lower $T_g$ value (-26.3℃). The decrease of $T_g$ value is because the cleavage reactions of coumarin groups in polymer chains result in the reduction of cross-link density. Such a reduction in $T_g$ can make the polymer chains easier to move, and may affect the healing process. After exposure to 365 nm UV light, a higher $T_g$ value (-18.1℃) is obtained due to the increase in cross-linking density resulting from the dimerization reaction of coumarin groups (Abdallh et al. 2017).

We also performed self-healing experiments on the as-prepared latex films with different CMA dosages. The films were scratched using a razor blade to study the self-healing property. The optical microscope images of the cut film before and after self-healing at different CMA dosages are shown in Fig. 12. It is obvious that all latex films exhibit a good healing ability, and the healing efficiency increases firstly with CMA dosage from 0 wt% to 3 wt%. After further increase of the CMA dosage, the healing efficiency is reduced. This may be because appropriate introduction of CMA groups into the polymer matrix can provide sufficient dynamic cross-linking points to allow for greater diffusion of the polymer chains at the fracture interface, which improves the healing efficiency (Qiu et al. 2016). However, when the CMA dosage is more than 3 wt%, the excessive CMA groups lead to a higher rigidity of the polymer chains, which may restrict the mobility of polymer chains in healing process, and weaken healability of the latex film (Hughes et al. 2019).

In addition, the controlled experiment was carried out to confirm the healing is owing to the dynamic bonds of coumarin moieties within polymer chains rather than the application of heat. As seen in Fig. 13b, when the sample is only exposed to the UV light there is no change in the damaged scratches. Compared to the sample exposed only to UV light, the scratches of the heated sample show

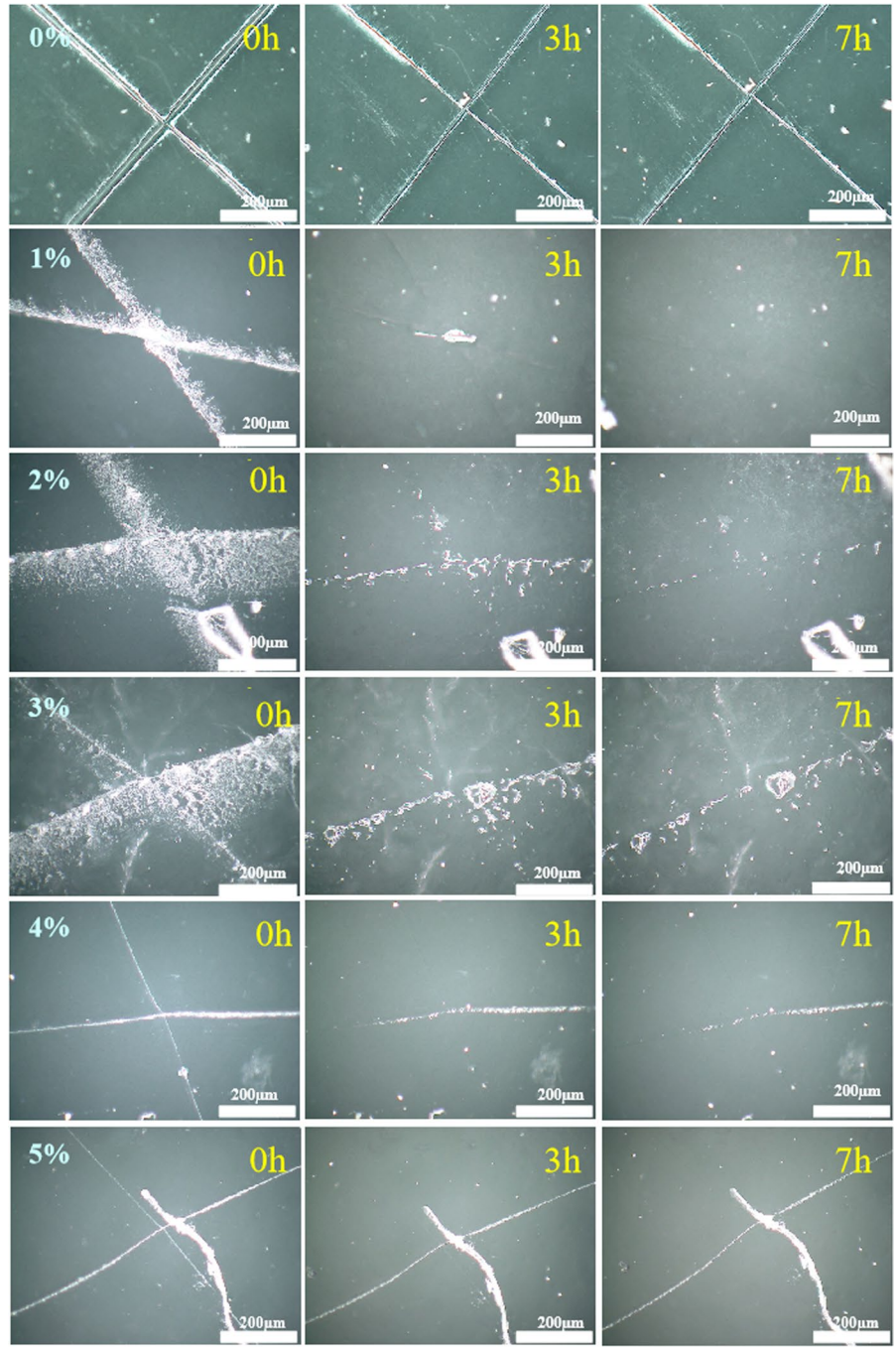


**Fig. 12** Optical micrographs of scratched latex films with different CMA dosages under the exposure of UV light at 100℃ for 0 h, 3 h, and 7 h

only small changes on the surface (Fig. 13c), indicating the healing requires photo-stimulated depolymerisation, in other words, healing is impossible without UV light to induce cleavage and recombination of coumarin moieties in polymer chains (Abdallh et al. 2019a). For the sample with a treatment of heat and UV light shows a noticeable healing effect (Fig. 13a). These results indicate that the thermal energy can encourage molecular mobility, but the healing requires to be triggered by UV light because of the photoreversible reaction of coumarin moieties (Abdallh et al. 2017).

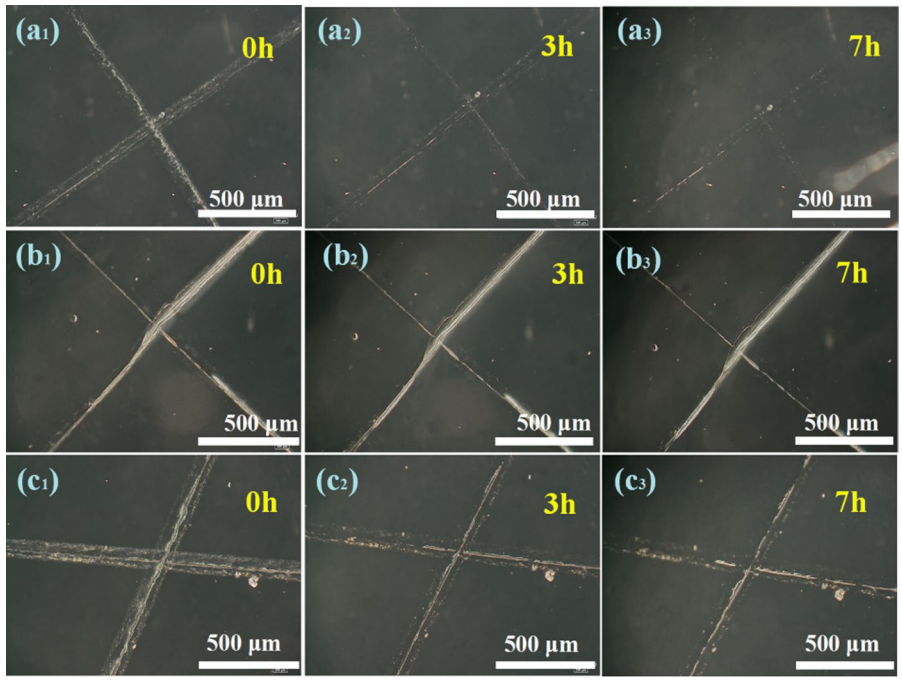


**Fig. 13** Scratched and healed latex films under UV light and heat treatment ($a_1$-$a_3$), under UV light treatment only ($b_1$-$b_3$), and under heat treatment only ($c_1$-$c_3$)

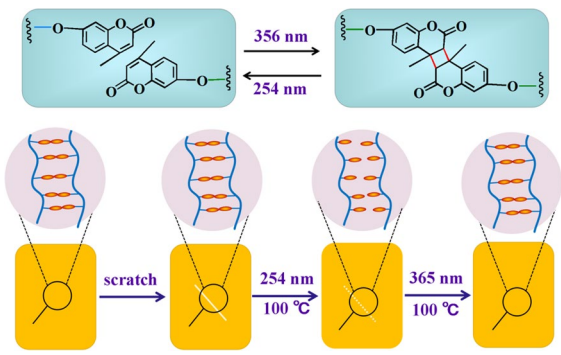


**Scheme 2** Schematic illustration of the self-healing process of the latex film

Based on the aforementioned experimental results, the self-healing mechanism of the latex film is schematically shown in Scheme 2. As stated previously, the coumarin moieties in the film can undergo the photoreversible dimerization reactions (Abdallh et al. 2019b). Firstly, light-responsive cellulose nanocrystal/fluorinated polyacrylate latex film is irradiated with 365 nm UV light to promote the coumarin dimerization reaction and form the crosslinked hard film. Subsequently, the latex film is scratched by a razor blade. When the latex film with scratches is irradiated with 254 nm UV light at 100℃, the depolymerisation reaction occurs and a softer film with the mobile uncrosslinked linear chains is formed. At the same time, the thermally-induced polymer chains move effectively, and flow into the scratch regions, which shortens the distance between two sides of the scratch and brings them closer to each other. Subsequent the latex film is exposed at 365 nm UV light to trigger the reformation of the crosslinks by coumarin dimers, promoting the reconnection between the damaged surfaces, and they fuse to become one piece and thus the scratch is healed.

## Conclusions

Coumarin functionalized waterborne light-responsive cellulose nanocrystal/fluorinated polyacrylate emulsion was synthesized successfully using light-responsive cellulose nanocrystal (CNC) particles as Pickering stabilizers via RAFT-mediated Pickering emulsion polymerization. The EDX result exhibited that the F element presented a gradient distribution along the latex film thickness in the depth direction. AFM result revealed that the UV irradiation at 365 nm could improve the roughness of the latex film. The resulting hydrophobic, oleophobic and mechanical properties of latex films could be easily

tuned by varying the dosage of CMA monomer and the wavelength of UV light. The tensile strength increased as the dosage of CMA increased from 0 to 4 wt%, and decreased afterwards with further increase in the CMA dosage. After the UV irradiation at 365 nm, the maximum tensile value increased from 3.0 MPa to 6.4 MPa, and the maximum water contact angle and $CH_2I_2$ contact angle increased by 6.1° and 2.3°, respectively. In addition, the reversible photo-dimerization reactivity of coumarin moieties in latex film was studied by FT-IR and DSC. The resultant latex film showed noticeable self-healing property after healing with 365 nm UV irradiation. The development of methods and materials in this work may provide a new insight into the fabrication of novel waterborne self-healing materials for extensive applications.

**Acknowledgments** We thank National Natural Science Foundation of China (No.21978162 and No.21206088), Key Research and Development Project of Xianyang City (2021ZDYF-GY-0037), Shaanxi Provincial Natural Science Foundation of China (No.2017JZ003), and Science and Technology Plan of Xi'an City (No. 2019216514GXRC001CG002-GXYD1.3) for supporting this research.

**Funding** This work was supported by the National Natural Science Foundation of China (No. 21978162 and No. 21206088), Key Research and Development Project of Xianyang City (2021ZDYF-GY-0037), Shaanxi Provincial Natural Science Foundation of China (No.2017JZ003), and Science and Technology Plan of Xi'an City (No. 2019216514GXRC001CG002-GXYD1.3).

**Declarations**

**Conflict of interest** There are no conflicts to declare.

## References

Abdallh M, Hearn MTW, Simon GP, Saito K (2017) Light triggered self-healing of polyacrylate polymers crosslinked with 7-methacryloyoxycoumarin crosslinker. Polym Chem 8:85875–85883. https://doi.org/10.1039/c7py01385j

Abdallh M, He P, Hearn MTW, Simon GP, Saito K (2019a) Light-switchable self-healing dynamic linear polymers: reversible cycloaddition reactions of thymine-containing units. ChemPlusChem 84:333–337. https://doi.org/10.1002/cplu.201900079

Abdallh M, Yoshikawa C, Hearn MTW, Simon GP, Saito K (2019b) Photoreversible smart polymers based on 2π+2π cycloaddition reactions: nanofilms to self-healing films. Macromolecules 52:2446–2455. https://doi.org/10.1021/acs.macromol.8b01729

Banerjee S, Tripathy R, Cozzens D, Nagy T, Keki S, Zsuga M, Faust R (2015) Photoinduced smart, self-healing polymer sealant for photovoltaics. ACS Appl Mater Inter 7:2064–2072. https://doi.org/10.1021/am508096c

Bian H, Yang Y, Tu P (2017) Crystalline structure analysis of all-cellulose nanocomposites films based on corn and wheat straw. Bioresources 16:8353–8365. https://doi.org/10.21203/rs.3.rs-511111/v1

Bonardd S, Robles E, Barandiaran I, Saldías C, Leiva Á, Kortaberria G (2018) Biocomposites with increased dielectric constant based on chitosan and nitrile-modified cellulose nanocrystals. Carbohyd Polym 199:20–30. https://doi.org/10.1016/j.carbpol.2018.06.088

Cai YB, Zou HW, Zhou ST, Chen Y, Liang M (2020) Room-temperature self-healing ablative composites via dynamic covalent bonds for high-performance applications. ACS Appl Polym Mater 2:3977–3987. https://doi.org/10.1021/acsapm.0c00638

Cao LM, Gong Z, Liu C, Fan JF, Chen YK (2021) Design and fabrication of mechanically strong and self-healing rubbers via metal-ligand coordination bonds as dynamic crosslinks. Compos Sci Technol 207:108750. https://doi.org/10.1016/j.compscitech.2021.108750

Fouconnier B, Lopez-Serrano F, Lee RIP, Terrazas-Rodriguez JE, Roman-Guerrero A, Barrera MC, Escobar J (2021) Hybrid microspheres and percolated monoliths synthesized via Pickering emulsion co-polymerization stabilized by in situ surface-modified silica nanoparticles. Express Polym Lett 15:554–567. https://doi.org/10.3144/expresspolymlett.2021.47

French AD (2013) Idealized powder diffraction patterns for cellulose polymorphs. Cellulose 21:885–896. https://doi.org/10.1007/s10570-013-0030-4

Guo HS, Han Y, Zhao WQ, Yang J, Zhang L (2020) Universally autonomous self-healing elastomer with high stretchability. Nat Commun 11:2037. https://doi.org/10.1038/s41467-020-15949-8

Han MS, Zhang XY, Li L, Peng C, Bao L, Ou EC, Xiong YQ, Xu WJ (2014) Dual-switchable surfaces between hydrophobic and superhydrophobic fabricated by the combination of click chemistry and RAFT. Express Polym Lett 8:528–542. https://doi.org/10.3144/expresspolymlett.2014.56

Hosseinzadeh B, Nikfarjam N, Kazemi SH (2021) Hollow molecularly imprinted microspheres made by w/o/w double Pickering emulsion polymerization stabilized by graphene oxide quantum dots targeted for determination of l-cysteine concentration. Colloid Surf a: Physicochem Eng Asp 612:125978. https://doi.org/10.1016/j.colsurfa.2020.125978

Hughes T, Simon GP, Saito K (2018) Improvement and tuning of the performance of light-healable polymers by variation of the monomer content. Polym Chem 9:5585–5593. https://doi.org/10.1039/c8py01203b

Hughes T, Simon GP, Saito K (2019) Photocuring of 4-arm coumarin-functionalised monomers to form highly photoreversible crosslinked epoxy coatings. Polym Chem 10:2134–2142. https://doi.org/10.1039/c8py01767k

Joseph JJP, Miglani C, Singh A, Gupta D, Pal A (2020) Photoresponsive chain collapse in flexo-rigid functional

copolymer to modulate self-healing behavio. Soft Matter 16:2506–2515. https://doi.org/10.1039/d0sm00033g
Kabb CP, Bryan CSO', Deng CC, Angelini TE, Sumerlin BS (2018) Photoreversible covalent hydrogels for soft-matter additive manufacturing. ACS Appl Mater Inter 10:16793–16801. https://doi.org/10.1021/acsami.8b02441
Li H, Zhou JH, Zhao JJ, Li YN, Lu K (2020) Synthesis of cellulose nanocrystals-armored fluorinated polyacrylate latexes via Pickering emulsion polymerization and their film properties. Colloid Surf B Biointerfaces 192:111071. https://doi.org/10.1016/j.colsurfb.2020.111071
Liu BF, Yang DC, Man H, Liu YQ, Xu H, Wang WX, Bai LJ (2017) A green Pickering emulsion stabilized by cellulose nanocrystals via RAFT polymerization. Cellulose 25:77–85. https://doi.org/10.1007/s10570-017-1559-4
Lin YL, Hu HW, Yi P, Sun S, Li YH, Liu XT, Li GJ (2020) Zwitterionic hydrogels formed via quadruple hydrogen-bonds with ultra-fast room-temperature self-healing ability. Mate Lett 269:127665. https://doi.org/10.1016/j.matlet.2020.127665
Liu AQ, Gao XY, Xie XL, Ma WJ, Xie M, Sun RY (2020) Stiffness switchable supramolecular hydrogels by photo-regulating crosslinking status. Dyes Pigments 177:108288. https://doi.org/10.1016/j.dyepig.2020.108288
Moorthy JN, Venkatesan K, Weisd RG (1992) Photodimerization of coumarins in solid cyclodextrin inclusion complexes. J Org Chem 57:3292–3297. https://doi.org/10.1021/jo00038a012
Morgen TO, Luttikhedde H, Mecking S (2019) Aqueous dispersions of ethylene copolymers and their laponite clay nanocomposites from free-radical dispersion polymerization. Macromolecules 52:4270–4277. https://doi.org/10.1021/acs.macromol.9b00305
Navarro R, Seoane-Rivero R, Cuevas JM, Marcos-Fernandez Á (2020) A novel strategy to polyurethanes with improved mechanical properties by photoactivation of amidocoumarin moieties. RSC Adv 10:29935–29944. https://doi.org/10.1039/d0ra06372j
Obi M, Morino S, Ichimura K (1999) Factors affecting photoalignment of liquid crystals induced by polymethacrylates with coumarin side chains. Chem Mater 11:656–664. https://doi.org/10.1021/cm980533v
Qiu T, Wang XJ, Lin XY, Zhu ZQ, Li XY, Guo LH (2016) Emulsion polymerization to synthesize self-healing films toward healing on fractures: a feasible strategy. J Polym Sci Part a: Polym Chem 54:3071–3078. https://doi.org/10.1002/pola.28217
Wang GL, Xi MZ, Bai LJ, Liang Y, Yang LX, Wang WX, Chen H, Yang HW (2019a) Pickering emulsion of metal-free photoinduced electron transfer-ATRP stabilized by cellulose nanocrystals. Cellulose 26:5947–5957. https://doi.org/10.1007/s10570-019-02528-4
Wang Y, Liu Q, Li JH, Ling L, Zhang GP, Sun R, Wong CP (2019b) UV-triggered self-healing polyurethane with enhanced stretchability and elasticity. Polymer 172:187–195. https://doi.org/10.1016/j.polymer.2019.03.045
Wei HT, Yang Y, Huang X, Zhu Y, Wang H, Huang GS, Wu JR (2020) Transparent, robust, water-resistant and high-barrier self-healing elastomers reinforced by dynamic supramolecular nanosheets with switchable interfacial connection. J Mater Chem A 8:9013–9020. https://doi.org/10.1039/d0ta01352h
Werner A, Schmitt V, Sèbe G, Héroguezl V (2019) Convenient synthesis of hybrid polymer materials by AGET-ATRP polymerization of Pickering emulsions stabilized by cellulose nanocrystals grafted with reactive moieties. Biomacromol 20:490–501. https://doi.org/10.1021/acs.biomac.8b01482
Wong CS, Hassan NI, Su'ait MS, Serra MAP, Gonzalez JAM, Granda LA, Badri KH (2019) Photo-activated self-healing bio-based polyurethanes. Ind Crop Prod 140:111613. https://doi.org/10.1016/j.indcrop.2019.111613
Xu XZ, Liu F, Jiang L, Zhu JY, Haagenson D, Wiesenborn DP (2013) Cellulose nanocrystals vs. cellulose nanofibrils: a comparative study on their microstructures and effects as polymer reinforcing agents. ACS Appl Mater Interfaces 5:2999–3009. https://doi.org/10.1021/am302624t
Yang SW, Du XS, Deng S, Qiu JH, Du ZL, Cheng X, Wang HB (2020) Recyclable and self-healing polyurethane composites based on Diels-Alder reaction for efficient solar-to-thermal energy storage. Chem Eng J 398:125654. https://doi.org/10.1016/j.cej.2020.125654
Yu LL, Xu KG, Ge LP, Wan WB, Darabi A, Xing M, Zhong W (2016) Cytocompatible, photoreversible, and self-healing hydrogels for regulating bone marrow stromal cell differentiation. Macromol Biosci 16:1381–1390. https://doi.org/10.1002/mabi.201500457
Yue YY, Han JQ, Han GP, Zhang QQ, French AD, Wu QL (2015) Characterization of cellulose I/II hybrid fibers isolated from energycane bagasse during the delignification process: morphology, crystallinity and percentage estimation. Carbohydr Polym 133:438–447. https://doi.org/10.1016/j.carbpol.2015.07.058
Zhai KK, Pei XP, Wang C, Deng YK, Tan Y, Bai YG, Zhang BC, Xu K, Wang PX (2019) Water-in-oil Pickering emulsion polymerization of n-isopropyl acrylamide using starch-based nanoparticles as emulsifier. Int J Biol Macromol 131:1032–1037. https://doi.org/10.1016/j.ijbiomac.2019.03.107
Zhang WJ, Hong CY, Pan CY (2017) Efficient fabrication of photosensitive polymeric nano-objects via an ingenious formulation of RAFT dispersion polymerization and their application for drug delivery. Biomacromol 18:1210–1217. https://doi.org/10.1021/acs.biomac.6b01887
Zhang BY, Zhang Z, Kapar S, Ataeian P, Bernardes JDS, Berry R, Zhao W, Zhou GF, Tam KC (2019) Microencapsulation of phase change materials with polystyrene/cellulose nanocrystal hybrid shell via Pickering emulsion polymerization. ACS Sustain Chem Eng 7:17756–17767. https://doi.org/10.1021/acssuschemeng.9b04134
Zhang YF, Yang H, Naren N, Rowan SJ (2020) Surfactant-free latex nanocomposites stabilized and reinforced by hydrophobically functionalized cellulose nanocrystals. ACS Appl Polym Mater 2:2291–2302. https://doi.org/10.1021/acsapm.0c00263
Zhang LY, Zhu LL, Chen YC (2021) Fabrication of carbon nanotubes/polystyrene nanocomposites via Pickering emulsion polymerization. Fuller Nanotub Car N 29:840–843. https://doi.org/10.1080/1536383x.2021.1909000

Zhou JH, Zhang L, Ma JZ (2013) Fluorinated polyacrylate emulsifier-free emulsion mediated by poly(acrylic acid)-b-poly(hexafluorobutyl acrylate) trithiocarbonate via ab initio RAFT emulsion polymerization. Chem Eng J 223:8–17. https://doi.org/10.1016/j.cej.2013.02.117

Zhou JH, Wang HL, Zhang L, Ma JZ (2014) Ab initio reversible addition-fragmentation chain transfer emulsion polymerization of styrene/butyl acrylate mediated by poly(acrylic acid)-block-polystyrene trithiocarbonate. Polym Int 63:2098–2104. https://doi.org/10.1002/pi.4755

Zhou JH, Duan H, Ma JZ, Ma YR (2015) Synthesis and characterization of nano-SiO2 modified fluorine-containing polyacrylate emulsifier-free emulsion. Appl Surf Sci 331:504–511. https://doi.org/10.1016/j.apsusc.2015.01.098

Zhou JH, He RY, Ma JZ (2016) RAFT-mediated polymerization-induced self-assembly of poly(acrylic acid)-b-poly(hexafluorobutyl acrylate): effect of the pH on the synthesis of self-stabilized particles. Polymers 8:207. https://doi.org/10.3390/polym8060207

Zhou JH, Wang XL, Li YN, Li H, Lu K (2020) Preparation of cellulose nanocrystal-dressed fluorinated polyacrylate latex particles via RAFT-mediated Pickering emulsion polymerization and application on fabric finishing. Cellulose 27:6617–6628. https://doi.org/10.1007/s10570-020-03227-1

Zhu MSQ, Jin HL, Shao T, Li YY, Liu J, Gan LH, Long MN (2020) Polysaccharide-based fast self-healing ion gel based on acylhydrazone and metal coordination bonds. Mater Design 192:108723. https://doi.org/10.1016/j.matdes.2020.108723